Inelastic rate coefficients for collisions of C4H-with H2

C. Balança, E. Quintas-Sánchez, R. Dawes, F. Dumouchel, François Lique, N. Feautrier

Monthly Notices of the ROYAL ASTRONOMICAL SOCIETY

MNRAS **508,** 1148–1155 (2021) https://doi.org/10.1093/mnras/stab2563
Advance Access publication 2021 September 11

Inelastic rate coefficients for collisions of C_4H^- with H_2

Christian Balança,[1]★ Ernesto Quintas-Sánchez,[2] Richard Dawes,[2] Fabien Dumouchel,[3] François Lique[1,3,4] and Nicole Feautrier[1]

[1]*Observatoire de Paris, Université PSL, CNRS-UMR 8112, LERMA, F-92195 Meudon, France*
[2]*Department of Chemistry, Missouri University of Science and Technology, Rolla, MO 65409, USA*
[3]*LOMC - UMR 6294, CNRS-Université du Havre, 25 rue Philippe Lebon, BP 1123, F-76063 Le Havre Cedex, France*
[4]*Univ Rennes, CNRS, IPR (Institut de Physique de Rennes) - UMR 6251, F-35000 Rennes, France*

Accepted 2021 August 30. Received 2021 August 23; in original form 2021 June 21

ABSTRACT

Carbon-chain anions were recently detected in the interstellar medium. These very reactive species are used as tracers of the physical and chemical conditions in a variety of astrophysical environments. However, the local thermodynamic equilibrium conditions are generally not fulfilled in these environments. Therefore, collisional as well as radiative rates are needed to accurately model the observed emission lines. We determine in this work the state-to-state rate coefficients of C_4H^- in collision with both *ortho*- and *para*-H_2. A new ab initio 4D potential energy surface was computed using explicitly correlated coupled-cluster procedures. This surface was then employed to determine rotational excitation and de-excitation cross-sections and rate coefficients for the first 21 rotational levels (up to rotational level $j_1 = 20$) using the close-coupling method, while the coupled-state approximation was used to extend the calculations up to $j_1 = 30$. State-to-state rate coefficients were obtained for the temperature range 2–100 K. The differences between the *ortho*- and *para*-H_2 rate coefficients are found to be small.

Key words: scattering – molecular data – molecular processes – ISM: abundances.

1 INTRODUCTION

Although the presence of anions in the interstellar medium (ISM) was predicted decades ago (Dalgarno & McCray 1973; Herbst 1981), the first detection of a negative ion, the C_6H^- linear carbon chain, is relatively recent (McCarthy et al. 2006). This is certainly due to the lack of laboratory spectroscopic data. Between 2006 and 2010, five new anions were detected: C_4H^- (Cernicharo et al. 2007; Agúndez et al. 2008; Sakai, Sakai & Yamamoto 2008), C_8H^- (Brünken et al. 2007; Kawaguchi et al. 2007; Remijan et al. 2007), CN^-(Agúndez et al. 2010), C_3N^- (Thaddeus et al. 2008), and C_5N^- (Cernicharo et al. 2008), all in IRC+10216 and TMC-1.

Carbon-chain anions play an important role in the chemical evolution in the ISM. However, the abundance of anions was found to be smaller by several orders of magnitude compared to their neutral parents, and nowadays chemical models cannot reproduce the observed anion-to-neutral ratio. In the cool low-density regions where anions are observed, the local thermodynamic equilibrium approximation is generally not valid and a proper modelling of the emission lines requires radiative and collisional rates with the most abundant species, which is H_2.

Collisional rate coefficients were published for the anionic carbon chains CN^- (Kłos & Lique 2011; collision with H_2), C_2H^- (Dumouchel et al. 2012; collision with He), C_6H^- (Walker et al. 2016, 2017; collision with He and H_2), and C_3N^- (Lara-Moreno, Stoecklin & Halvick 2019; collision with H_2). Very recently, collisional rate coefficients for C_4H^- in collision with *para*-H_2 ($j_2 = 0$) were calculated using a 2D potential energy surface (PES) built as an average of the 4D C_4H^-–H_2 interactions over different orientations of the H_2 molecule (Senent et al. 2019). However, no collisional data were generated for the *ortho*-H_2 colliders, whereas the C_4H^- anion is detected in media where the *ortho*-H_2 abundance is found to be relatively large (Cernicharo et al. 2007). Therefore, it seems useful to calculate C_4H^-–H_2 rate coefficients using a 4D PES, necessary to obtain both *ortho*- and *para*-H_2 rate coefficients.

In this paper, we report the first 4D C_4H^-–H_2 interaction PES and inelastic rate coefficients for C_4H^- in collision with both *ortho*- and *para*-H_2. The ab initio PES was computed using explicitly correlated coupled-cluster-based procedures. Quantum-scattering calculations based on the close-coupling (CC) method were performed to compute rotational excitation rate coefficients for the first 21 rotational levels of C_4H^- while the coupled-states (CS) approximation was used to extend the calculations to the first 30 rotational levels. Cross-sections were calculated for collisional energies up to 1000 cm^{-1}, leading to de-excitation rate coefficients for temperatures up to 100 K.

Details of the electronic structure calculations are given in Section 2. Section 3 provides a brief description of the scattering calculations. Section 4 presents collisional cross-sections and rate coefficients, and conclusions are given in Section 5.

2 POTENTIAL ENERGY SURFACE

The coordinates used to define the 4D C_4H^-–H_2 PES are illustrated in Fig. 1. $\vec{r}_1$ and $\vec{r}_2$ are vectors aligned with the fragments. Coordinate R is the centre-of-mass separation, while θ_1 and θ_2 are the angles between $\vec{R}$ and the vectors $\vec{r}_1$ and $\vec{r}_2$ (respectively). φ is the dihedral

★ E-mail: Christian.Balanca@obspm.fr

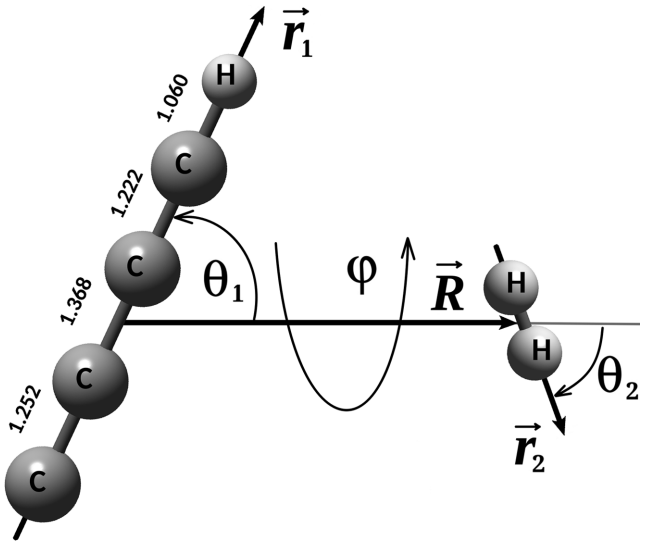

Figure 1. Coordinates used to describe the C_4H^-–H_2 interaction. R: centre-of-mass separation (length of $\vec{R}$); θ_1 and θ_2: angles between $\vec{R}$ and the vectors $\vec{r}_1$ and $\vec{r}_2$; and φ: torsional angle. The employed bond distances for the linear C_4H^- molecule are given in Å (see text).

(out-of-plane) torsional angle. Note that for $\theta_1 = 0^\circ$ the C_4H^- molecule aligns with the H atom pointing to the H_2 molecule.

2.1 Electronic structure calculations

All ab initio calculations were performed using the MOLPRO electronic structure code package (Werner et al. 2012). The non-bonded interaction energies were computed using explicitly correlated coupled-cluster theory (Knizia, Adler & Werner 2009; Werner, Knizia & Manby 2011). Each energy was computed with the fragments interacting as a supersystem at the CCSD(T)-F12b/VTZ-F12 level, without basis extrapolation or counterpoise correction (on the basis of preliminary radial test cuts used to explore sensitivity to basis set completeness). In these tests, the Complete Basis Set (CBS) limit was estimated by extrapolating results from the VTZ-F12 and VQZ-F12 bases using the l^{-3} formula. At the global minimum (GM), the well depth for VTZ-F12 was found to be very close to the CBS value (-793.5 and $-794.9\,\mathrm{cm}^{-1}$, respectively), and differences at geometries extending towards the long range are considerably smaller. We rationalize the lack of strong basis set dependence for this anionic system as being due to the closed-shell nature of the anion. Core electrons were excluded from the correlation treatment.

As the lowest bending mode, ν_7, equal to $214\,\mathrm{cm}^{-1}$ (Senent & Hochlaf 2010), is well above the highest C_4H^- rotational level considered in this work, the result of previous work (Denis-Alpizar et al. 2013; Balança et al. 2018) supports the expectation of a relatively small impact of (closed) vibrational channels for pure rotational excitation.

The bond distance for H_2 was fixed at $r_{HH} = 0.766\,65$ Å, the vibrationally averaged bond distance for the ground ro-vibrational state of H_2. For C_4H^-, the equilibrium geometry is linear and the structure employed in this study was that obtained by optimization at the same level as the high-level PES; the employed bond distances are shown in Fig. 1. To guide the placement of high-level data toward energetically accessible regions, a lower level guide surface was first constructed at the CCSD(T)-F12a/VDZ-F12 level of theory.

2.2 Analytical representation

As we have done in the past for other van der Waals linear dimers (Dawes et al. 2010; Brown et al. 2012; Dawes, Wang & Carrington 2013; Brown et al. 2014; Donoghue et al. 2016; Wang, Carrington & Dawes 2016; Barclay et al. 2018; Bop et al. 2019; Castro-Juárez et al. 2019; Desrousseaux et al. 2019, 2021a; Quintas-Sánchez et al. 2020), the PES analytical representation was constructed using an automated interpolating moving least squares methodology, freely available as a software package under the name AUTOSURF (Quintas-Sánchez & Dawes 2019). This interpolative approach can accommodate arbitrary energy-surface topographies and is advantageous for PESs with large anisotropy, which are challenging for traditional quadrature-type expansions (Dawes & Quintas-Sánchez 2018). The shortest intermonomer centre-of-mass distance considered is $R = 2.3$ Å, with the additional restriction of a maximum repulsive energy of 6 kcal/mol ($\sim 2100\,\mathrm{cm}^{-1}$) above the separated monomers' asymptote. The initial lower level guide surface was constructed using a set of 3441 symmetry-unique points, distributed using a Sobol sequence (Sobol 1976) biased to sample the short-range region more densely. For the high-level PES, the global estimated root-mean-squared fitting error tolerance was set to $0.33\,\mathrm{cm}^{-1}$ for energies below the asymptote, and the total number of automatically generated symmetry-unique points needed to reach that target was 5122. The ab initio data coverage in the fitted PES extends to $R = 22$ Å.

Fig. 2 shows a 2D cut of the PES as a function of θ_1 and θ_2 for planar configurations ($\varphi = 0^\circ$). The plot describes the complete ranges of θ_1 and θ_2 relaxing coordinate R for each pair of angles. Stationary points and transition structures (TSs) are also highlighted in the figure. The PES is characterized by a single minimum (the two molecules aligned, with the H_2 at the C-end of the C_4H^- molecule), with a well depth of $793.5\,\mathrm{cm}^{-1}$ and a centre-of-mass separation of $R = 5.027$ Å. The energies and geometric parameters of the GM and the TS between equivalent minima (cf. Fig. 2) are given in Table 1.

Fig. 3 shows the potential as a function of R upon approach from different angular poses, giving some indication of the anisotropy of the interactions. It is worth highlighting that none of the ab initio energies plotted in Fig. 3 were used in the PES-construction process, and thus serve to confirm the overall quality of our fitted potential. In order to better appreciate the anisotropy of the interaction with respect to C_4H^- and H_2 rotations, additional 2D plots of the PES are shown in Fig. 4. The plots in Fig. 4 explore the end-on ($\theta_2 = 0^\circ$) and side-on ($\theta_2 = 90^\circ$) approach of the H_2 fragment for planar configurations ($\varphi = 0^\circ$). A strong dependence of the PES on the orientation of the H_2 fragment could contribute to different scattering dynamics for *para*- and *ortho*-H_2.

In previous work by Senent et al. (2019), rotational rate coefficients were obtained for C_4H^- in collision with *para*-H_2 using a PES averaged over five H_2 orientations. When building their 2D PES and testing the electronic structure calculations, a minimum of $-780.27\,\mathrm{cm}^{-1}$ was found in the collinear orientation of the two species at a distance of 5.026 Å. This minimum has characteristics very close to those obtained for the GM of our 4D PES (cf. Table 1). However, the PES for positions of H_2 about the C_4H^- fragment changes qualitatively in the averaging, and a minimum with a depth of only $-301.54\,\mathrm{cm}^{-1}$ was found at $\theta_1 = 90^\circ$ (at the side of C_4H^-) in the resulting 2D PES at $R = 3.17$ Å. To facilitate comparison, we used our 4D PES to construct a 2D averaged PES using the same 5-point formula as Senent et al. (2019; plotted in Fig. 5). The well depth of our 2D averaged PES is slightly deeper ($-336.2\,\mathrm{cm}^{-1}$), while the geometry of the minimum is very similar (parameters are given in Table 1). These differences are due to the higher level of electronic

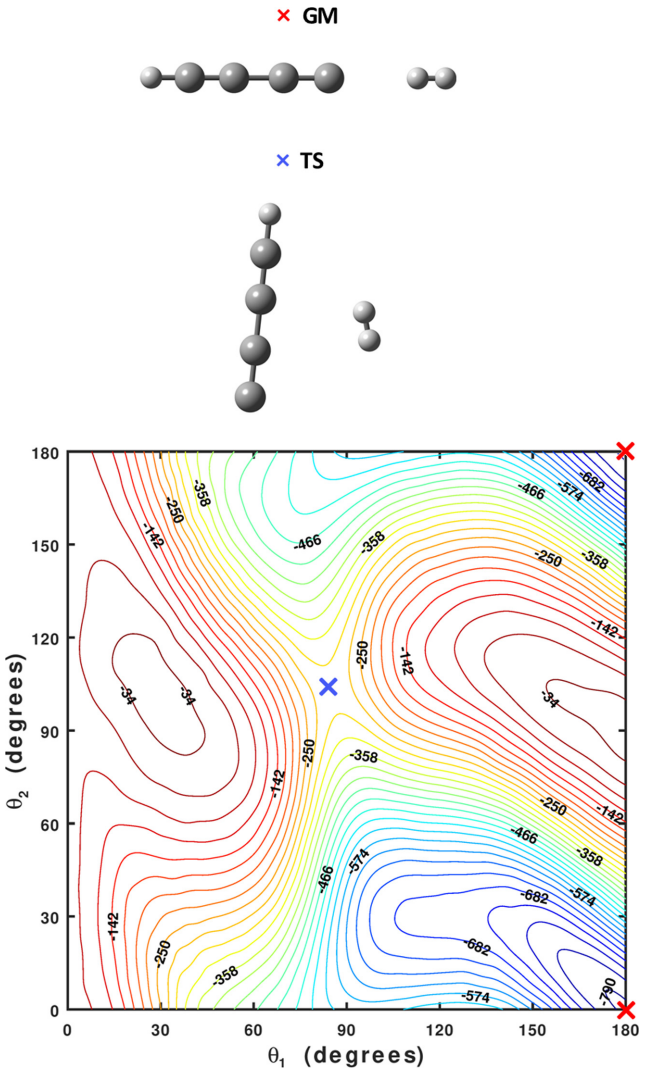

Figure 2. *R*-optimized contour plot of the PES as a function of the angles θ_1 and θ_2 for planar configurations ($\varphi = 0°$). For each pair of angles, the energy (given in cm^{-1}) is optimized with respect to the centre-of-mass distance *R*. The positions of stationary points – and the corresponding molecular configurations – are also highlighted.

Table 1. Geometric parameters and potential energy for the GM and TS of the $C_4H^- - H_2$ complex. The corresponding parameters for the GM of the averaged 2D PES (GM_{2D}) are also included (see text). Units are Angstroms, degrees, and cm^{-1}.

	GM	TS	GM_{2D}
R	5.027	3.136	3.197
θ_1	180.0	85.2	90.0
θ_2	0.0	103.1	–
φ	0.0	0.0	–
V	– 793.5	– 295.5	– 336.2

structure theory employed presently. As scattering calculations for *para*-H_2 are restricted to H_2, $j_2 = 0$ (see Section 3), the differences between Senent et al. and present rate coefficients are only due to the differences in the PES, not in the scattering methodology. The difference in the well depths of the two 2D potentials could affect the position and the shape of the resonances present at low kinetic

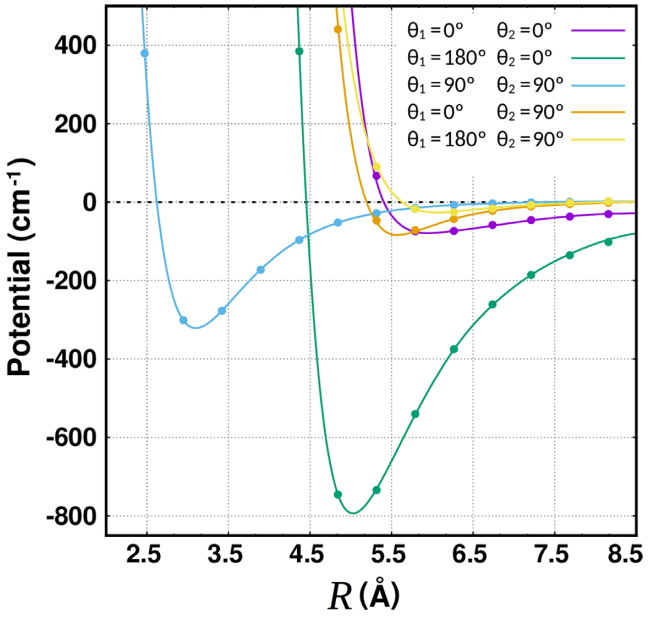

Figure 3. The energy along various radial cuts – defined by different relative orientations (θ_1, θ_2) of the monomers – is plotted for planar configurations ($\varphi = 0°$); thus illustrating the significant anisotropy of the PES. Lines represent the fitted PES, points represent ab initio calculations (not used in the fit).

energies but the global energy variations of the cross-sections are very similar, leading to small differences in the respective rate coefficients upon energy averaging.

Fundamentally, since asymptotically the rotational wavefunction for H_2 in $j_2 = 0$ is a constant (has no angular preference), the C_4H^- fragment really does *see* the approach of the H_2 molecule in an averaged way, which is much different than features of the 4D PES would suggest. Given this extreme quantum delocalization, an interesting aside would be to consider whether classical trajectories can realistically treat the scattering process (perhaps better in two dimensions than four?). Of course in a fully quantum treatment, in the close-interaction region this asymptotic representation starts to break down and higher channels ($j_2 > 0$) may need to be included for precise results.

3 SCATTERING CALCULATIONS

We consider in this article the collisions of C_4H^- with *para*- and *ortho*-H_2 described by:

$$C_4H^-(j_1) + H_2(j_2) \rightarrow C_4H^-(j_1') + H_2(j_2), \quad (1)$$

where j_1 and j_2 are the rotational angular momenta of C_4H^- and H_2, respectively. The calculations were performed for collisional energies in the range $0.1\,cm^{-1} \leq E_c \leq 1000\,cm^{-1}$, which allows a converged calculation of the rate coefficients for temperatures up to 100 K. The rotational energy levels of C_4H^-, shown in Table 2, were computed using the experimental rotational constants of Amano (2008): $B_0 = 0.1552722$, $D_0 = 0.196 \times 10^{-7}$, and $H_0 = -3.1 \times 10^{-15}\,cm^{-1}$.

Due to the strong anisotropy of the C_4H^-–H_2 PES at short intermolecular distances – that leads to steric hindrance and singularities in the angular expansion – we adopted the regularization procedure proposed by Wernli et al. (2007). The anisotropy of the PES is thus artificially reduced at very high energies by applying

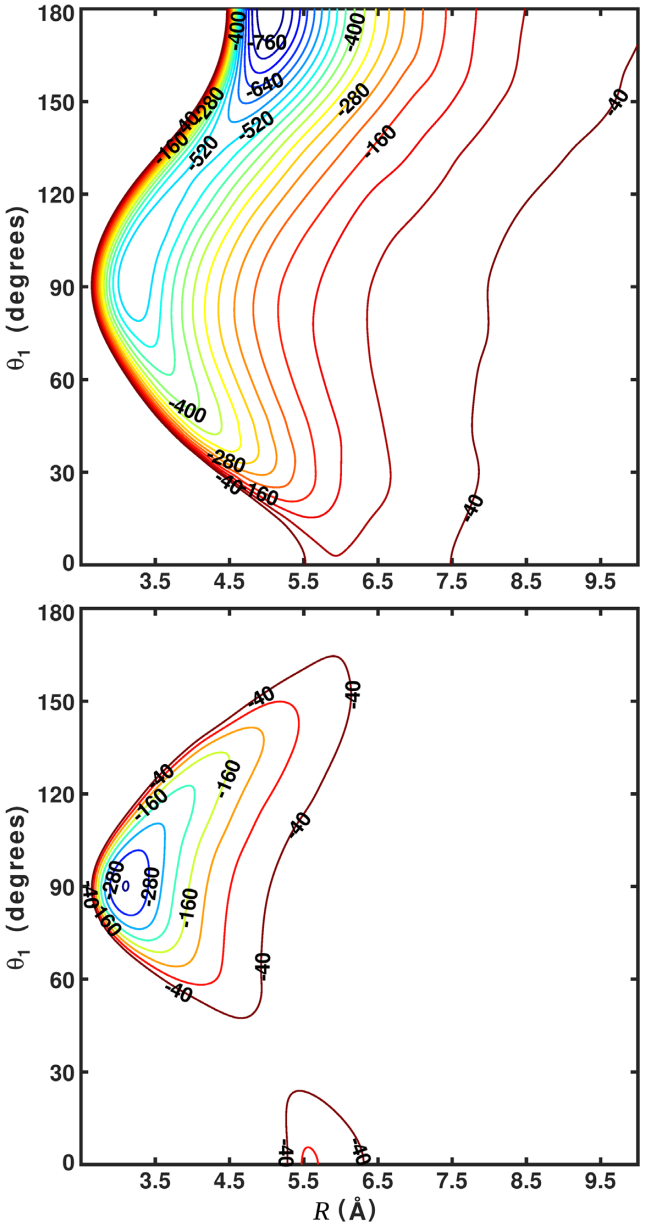

Figure 4. Contour plots of the PES (for energies below $-40\,\mathrm{cm}^{-1}$) showing the highly anisotropic potential for C_4H^- interacting with H_2. Upper panel: the plot of end-on approach of the H_2 fragment ($\theta_2 = 0°$) as a function of the intermonomer distance R and the orientation of C_4H^- illustrates the collinear well for approach of H_2 to the C-atom end ($\theta_1 = 180°$, see text). Lower panel: the plot of the side-on approach of H_2 ($\theta_2 = 90°$, $\phi = 0°$) shows, in contrast, the strong dependence of the interaction on the orientation of H_2.

a scaling factor such that the regularized PES remains identical to the original potential at low energies, but above a threshold energy V_a tends smoothly to a constant limit value based on the parameter V_b.

We have selected the parameters $V_a = 300\,\mathrm{cm}^{-1}$ and $V_b = 2000\,\mathrm{cm}^{-1}$. With these values, the regularized PES coincides with the original one for interaction energies below $300\,\mathrm{cm}^{-1}$, it is extremely accurate up to $500\,\mathrm{cm}^{-1}$, and smoothly saturates to a maximum value of $990\,\mathrm{cm}^{-1}$. It should be noted that this regularized PES should not be used for high collision energy calculations. For R distances larger than 22 Å, the PES is smoothly connected to an R^{-3} extrapolation.

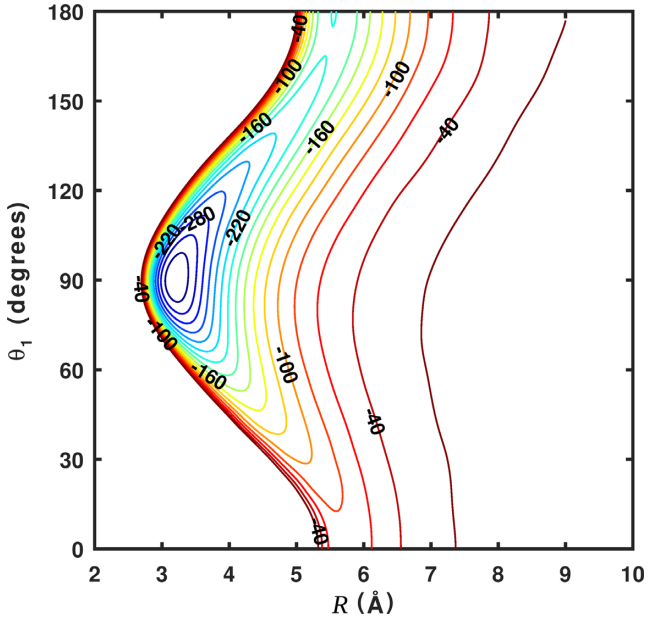

Figure 5. A plot is provided of a 2D averaged PES constructed by evaluating the full 4D PES using the same 5-point formula reported by Senent et al. (2019), see text.

Table 2. C_4H^- rotational energy levels (in cm^{-1}) obtained from the experimental rotational constants of Amano (2008).

j_1	ϵ_{j_1} (cm^{-1})	j_1	ϵ_{j_1} (cm^{-1})
0	0.000	21	71.732
1	0.311	22	78.563
2	0.932	23	85.704
3	1.863	24	93.156
4	3.105	25	100.919
5	4.658	26	108.851
6	6.521	27	117.216
7	8.695	28	125.889
8	11.179	29	134.871
9	13.974	30	144.162
10	17.080	31	153.760
11	20.496	32	163.667
12	24.222	33	173.881
13	28.259	34	184.403
14	32.606	35	195.233
15	37.264	36	206.370
16	42.233	37	217.814
17	47.511	38	229.565
18	53.101	39	241.623
19	59.000	40	253.988
20	65.211	–	–

Computation of collisional cross-sections was performed using the MOLSCAT nonreactive scattering code (Hutson & Green 1994). The modified log-derivative Airy propagator of Alexander & Manolopoulos (1987) was used to solve the scattering equations from $R = 2$ to $R = 42$ Å at low energies, with a decrease in maximum propagation to $R = 22$ Å for the highest energies. The rotational excitation rate coefficients $k_{j_1 \to j_1'}(T)$ were obtained for temperatures up to 100 K by averaging the computed cross-sections $\sigma_{j_1 \to j_1'}(E)$

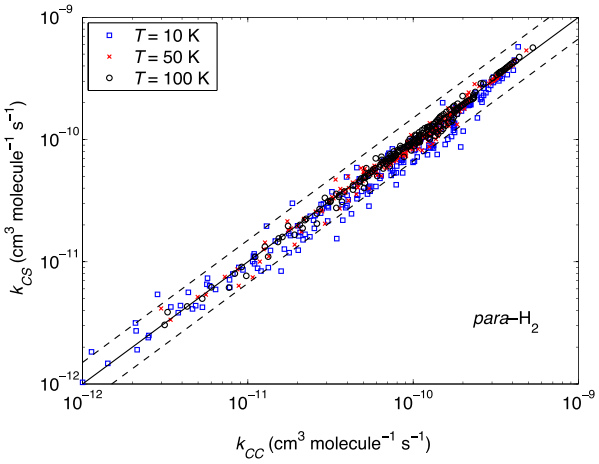

Figure 6. Comparison of the rate coefficients between the 15 first C_4H^- rotational levels for collisional de-excitation rate coefficients of C_4H^- by *para*-H_2 obtained at the CS approximation and those obtained at the CC level. The two dashed lines delimit the region where the rate coefficients differ by less than a factor of 1.5.

as:

$$k_{j_1 \to j_1'}(T) = \left(\frac{8k_BT}{\pi\mu}\right)^{\frac{1}{2}} \left(\frac{1}{k_BT}\right)^2 \times \int_0^\infty E_k\, \sigma_{j_1 \to j_1'}(E_k)\, e^{\frac{-E_k}{k_BT}} dE_k, \quad (2)$$

where $E_k = E - \epsilon_{j_1}$ is the relative kinetic energy, $\mu = 1.9336023$ is the reduced mass of C_4H^-–H_2, and k_B is the Boltzmann constant. The rate coefficients for the reverse transitions are given by the detailed balance relation.

The interaction potential $V(R, \theta_1, \theta_2, \varphi)$ was expanded over a suitable basis of angular functions for any intermolecular distance R (Green 1975):

$$V(R, \theta_1, \theta_2, \varphi) = \sum_{l_1 l_2 l} v_{l_1 l_2 l}(R) A_{l_1 l_2 l}(\theta_1, \theta_2, \varphi), \quad (3)$$

where $v_{l_1 l_2 l}(R)$ are the radial coefficients, and the angular basis functions $A_{l_1 l_2 l}(\theta_1, \theta_2, \varphi)$ are contracted normalized spherical harmonics. The angular expansion of the PES was carefully analysed. It was found that a PES expansion up to order $l_1^{max} = 40$ for C_4H^- and up to $l_2^{max} = 4$ for H_2 reproduces correctly the interaction. This l_1^{max} value was retained as it leads to cross-sections converged to better than 5 per cent from the results obtained with $l_1^{max} = 50$ and avoids prohibitively expensive calculations.

The fully quantal CC approach of Green (1975) was used to compute state-to-state cross sections between all rotational levels up to $j_1 = 20$. For $21 \leq j_1 \leq 30$, the CS approximation (McGuire & Kouri 1974) was employed since the numerical solution of CC calculations become prohibitive due to the large basis set needed for convergence. The validity of the CS approach was also tested. Fig. 6 displays CS C_4H^-–*para*-H_2 rate coefficients as a function of the CC ones at 10, 50, and 100 K. It was found that the CS approach can lead to inaccuracies of 20–50 per cent at low temperatures (10 K) whereas the two methods tend to agree within 10–30 per cent at higher temperatures (50 K).

The large well depth of the PES and the small value (0.155 cm^{-1}) of the rotational constant of C_4H^- imply that large basis sets are needed for convergence. Thus, rotational levels up to $j_1 = 25$ and $j_1 = 40$ were included into the C_4H^- basis set to obtain converged excitation cross-sections between the 21 and 30 first rotational levels, respectively. The H_2 rotational basis included only *para*-H_2 ($j_2 = 0$) and *ortho*-H_2 ($j_2 = 1$) levels. For different C_4H^- rotational transitions, Table 3 displays the convergence of the *para*-H_2 cross-sections calculated at a total energy of 100 cm^{-1} as a function of the (j_1^{max}, j_2^{max}) values in the basis sets. The addition of the H_2 ($j_2 = 2$) level in the basis set, led to cross-sections that are within 10 per cent (on average) of the values obtained using only the H_2 ($j_2 = 0$) level. Hence, only H_2 ($j_2 = 0$) and H_2 ($j_2 = 1$) were included in the basis. Hereafter, *para*- and *ortho*-H_2 refer to H_2 ($j_2 = 0$) and H_2 ($j_2 = 1$), respectively.

Table 3. Convergence of the rotational bases expressed as (j_1^{max}, j_2^{max}). Cross-sections ($\times 10^{-16}$ cm^2).

Transition $j_1 \to j_1'$	25,0	25,2	30,0	30,2	40,0	40,2
$1 \to 0$	18.77	18.70	18.88	16.53	18.89	16.70
$2 \to 0$	5.38	4.30	5.66	5.50	5.68	5.28
$2 \to 1$	25.90	28.27	25.20	28.07	25.21	27.52
$5 \to 4$	33.16	35.16	32.70	33.98	32.84	35.22
$10 \to 5$	6.28	7.02	6.38	7.52	6.26	7.02
$10 \to 9$	37.34	38.43	38.11	39.43	37.45	41.75
$15 \to 10$	7.61	9.42	7.94	9.67	7.55	8.97
$15 \to 14$	42.08	40.81	41.62	43.25	43.47	45.23

4 RESULTS

State-to-state inelastic rate coefficients are displayed in Fig. 7 for collisions of C_4H^- with both *para*- and *ortho*-H_2. After a rapid decrease at very low temperature, the rate coefficients for these selected $\Delta j_1 = -1$ transitions exhibit rather constant values and then increase slowly with temperature. Such quasi-constant values are expected for *para*-H_2 collisions according to the Langevin theory for ion–neutral interactions. The propensity rules for these rotational transitions are also interesting to consider. Fig. 8 shows the de-excitation rate coefficients at $T = 50$ K out of initial state $j_1 = 15$ for collisions with *para*- and *ortho*-H_2. The rate coefficients decrease continuously with increasing Δj_1, showing a strong propensity for $\Delta j_1 = -1$.

An important result is the high similarity shown in both Figs 7 and 8 between *para*- and *ortho*-H_2 rates. This similarity is observed at all temperatures, as shown in Fig. 9, which compares *ortho*- and *para*-H_2 de-excitation rate coefficients at 10, 50, and 100 K for all transitions involving the first 16 rotational levels. Difference between the two sets of data is rather small (less than 50 per cent). The agreement improves, with differences less than 10 per cent for the highest values, corresponding to transitions with the smallest Δj_1. Similar behaviour has also been observed in H_2 collisions with other ions, such as CN^- (Kłos & Lique 2011), C_6H^- (Walker et al. 2017), C_3N^- (Lara-Moreno et al. 2019), HCO^+ (Massó & Wiesenfeld 2014), N_2H^+ (Balança et al. 2020), and CF^+ (Desrousseaux et al. 2021b). As previously discussed by Walker et al. (2017), this close agreement between *para*- and *ortho*-H_2 rates shows that at the considered temperatures, effects of the long-range part of the interaction outweigh those of the short-range part. Anisotropies in the PES at short intermolecular distances mostly affect transitions with large Δj_1, leading to relatively small rate coefficients.

Fig. 10 presents a comparison between rate coefficients of C_4H^- in collision with *para*-H_2 obtained in this work and those obtained with a PES averaged over H_2 orientation (Senent et al. 2019). The agreement between the two sets of data is good, with differences lower than 10 per cent for the most dominant transitions. Such

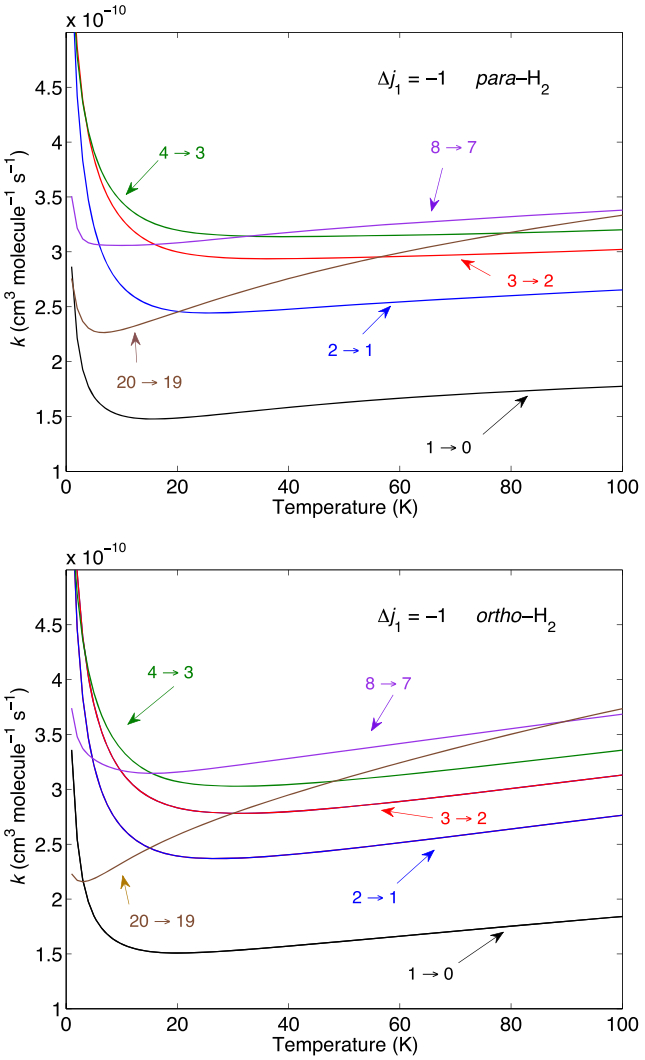

Figure 7. State-to-state rate coefficients for the rotational de-excitation of C_4H^- by *para*-H_2 and *ortho*-H_2 for selected $\Delta j_1 = -1$ transitions as a function of temperature. The rate coefficients are labelled according to the related $j_1 \rightarrow j_1'$ transition between the rotational states of C_4H^-.

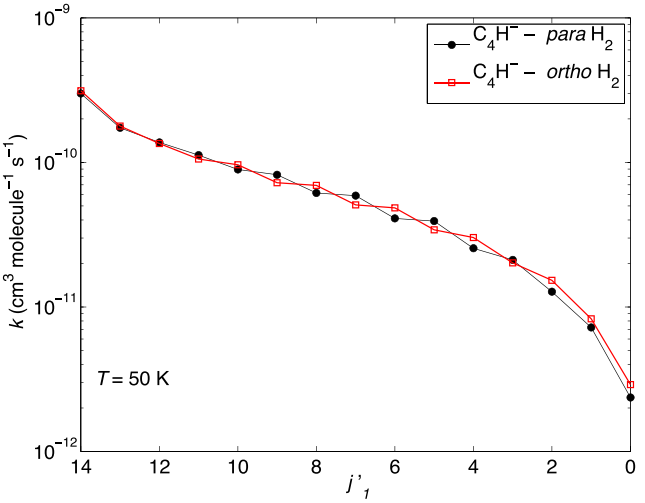

Figure 8. Propensity rule for transitions out of initial state $j_1 = 15$ for C_4H^- in collision with *para*- and *ortho*-H_2 at 50 K.

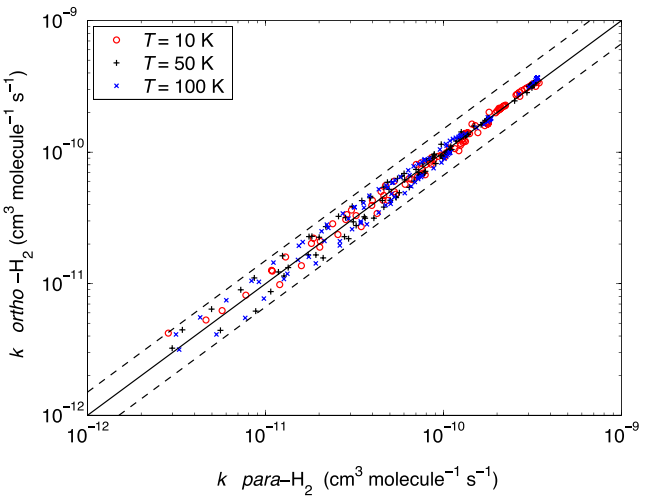

Figure 9. Comparison at 10, 50, and 100 K between rate coefficients for the collisional de-excitation of C_4H^- by *para*- and *ortho*-H_2. The two dashed lines delimit the region where the rate coefficients differ by less than a factor of 1.5.

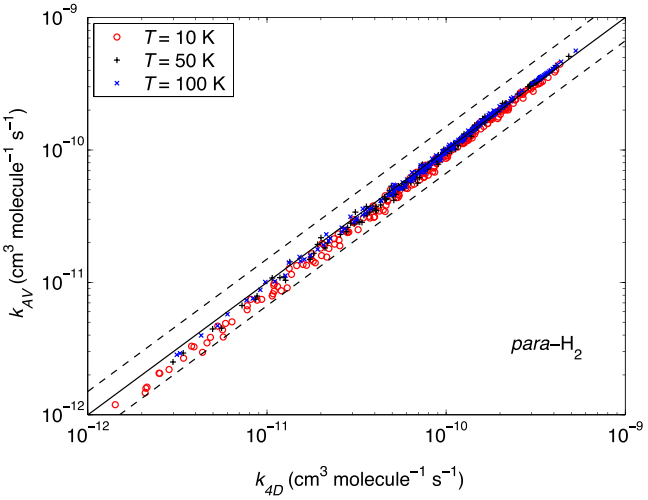

Figure 10. Comparison between the CC rate coefficients for collisional de-excitation of C_4H^- by *para*-H_2 obtained in this work (k_{4D}) and those (k_{AV}) obtained with a PES averaged over H_2 orientation (see text). The two dashed lines delimit the region where the rate coefficients differ by less than a factor of 1.5.

agreement was also found for rotational excitation of HCO^+ by *para*-H_2. It is shown that the 4D PES calculations (Massó & Wiesenfeld 2014; Denis-Alpizar et al. 2020) are in excellent agreement with those obtained by Yazidi, Ben Abdallah & Lique (2014) with an averaged 2D PES. This confirms the relatively small contribution of the H_2 orientation in the dynamics of collision for those ionic systems at low temperatures.

We consider now the comparison of the rotational transition rate coefficients obtained in this work for C_4H^-–H_2 with those obtained for other large anionic chains such as C_6H^- and C_3N^-. For all three systems, the PESs are not much different, with the GM observed in a collinear configuration and well-depth values in the range 700–800 cm^{-1}. Fig. 11 shows the *para*-H_2 rate coefficients at $T = 50$ K (upper panel) and $T = 100$ K (lower panel) for the de-excitation transition from the initial state $j_1 = 15$. As can be seen in the figure,

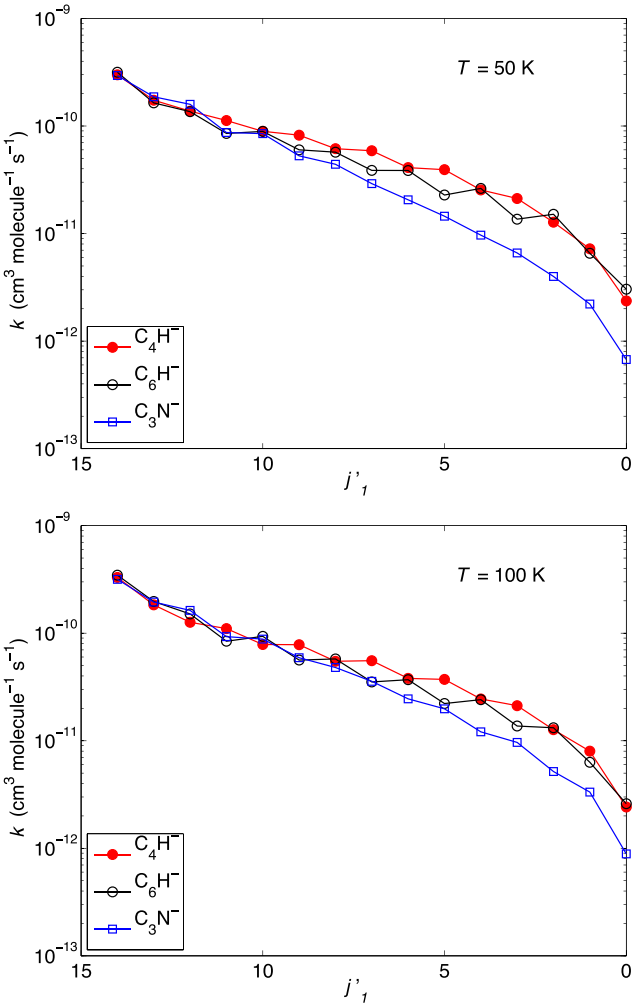

Figure 11. The *para*-H_2 de-excitation rate coefficients out of initial state $j_1 = 15$ of C_4H^- (this work), C_6H^- (Walker et al. 2017), and C_3N^- (Lara-Moreno et al. 2019) for $T = 50$ K and $T = 100$ K as a function of the final state j_1'.

the rate coefficients for the three systems are in good agreement for transitions with $\Delta j_1 \leq 5$. For larger Δj_1 values, the C_4H^- and C_6H^- rate coefficients are very similar, with remarkable agreement for the even j_1' values and small differences for the odd j_1' values, whereas the C_3N^- rate coefficients become progressively smaller. An explanation for these different behaviours could come from differences in angular anisotropy of the PESs at short intermolecular distances.

5 SUMMARY AND CONCLUSION

A new accurate 4D PES for the C_4H^-–H_2 system has been calculated at the (CCSD(T)-F12b/VTZ-F12) level of theory. This PES has a large well depth and exhibits strong anisotropies at short intermolecular distances. Rotational rate coefficients for collisions with *para*- and *ortho*-H_2 have been computed for temperatures ranging from 2 to 100 K for the first 21 rotational levels of C_4H^- using the CC method, while the CS approximation was used to extend the results for levels up to $j_1 = 30$.

The analysis of the results shows several important results: first of all, both *para*- and *ortho*-H_2 rate coefficients have dominant values for $\Delta j_1 = -1$ and decrease slowly for increasing Δj_1. Notably, strong similarities between the rate coefficients for collisions with *para*- and *ortho*-H_2 were found, in agreement with what was obtained for other ionic systems. Furthermore, the rotational rate coefficients computed for collisions with *para*-H_2 are in good agreement with those calculated by Senent et al. (2019) using a 2D PES. This behaviour has been also found for other ionic systems (Denis-Alpizar et al. 2020).

The rotational de-excitation rate coefficients for transitions out of the $j_1 = 15$ level compare well with those obtained for other large anionic chains (C_6H^- and C_3N^-). The agreement is remarkably good for $\Delta j_1 \leq 5$, and thus confirms the dominant effects of the long-range part of the interaction at the considered temperatures for these transitions.

ACKNOWLEDGEMENTS

This work was supported by the CNRS programs 'Physique et Chimie du Milieu Interstellaire (PCMI)' co-funded by the 'Centre National d'Etudes Spatiales (CNES)' and 'Programme National de Physique Stellaire (PNPS)'. Parts of the calculations were performed using HPC resources from GENCI-(CINES/IDRIS) (grant no. 2010040883) and work stations at the 'Centre Informatique' of Paris observatory. This work was also granted access to the HPC resources of MesoPSL financed by the 'Région Île de France' and the project Equip@Meso (reference ANR-10-EQPX-29-01) of the 'programme Investissements d'Avenir' supervised by the 'Agence Nationale pour la Recherche'. RD and EQ-S are supported by the US Department of Energy (Award DE-SC0019740). Computing resources were supported by the National Science Foundation under grant no. OAC-1919789.

DATA AVAILABILITY

The resulting rate coefficients will be made available in the LAMBDA (Schöier et al. 2005) and BASECOL (Dubernet et al. 2013) data bases.

REFERENCES

Agúndez M. et al., 2010, A&A, 517, L2
Agúndez M., Cernicharo J., Guélin M., Gerin M., McCarthy M. C., Thaddeus P., 2008, A&A, 478, L19
Alexander M. H., Manolopoulos D. E., 1987, J. Chem. Phys., 86, 2044
Amano T., 2008, J. Chem. Phys., 129, 244305
Balança C., Dayou F., Faure A., Wiesenfeld L., Feautrier N., 2018, MNRAS, 479, 2692
Balança C., Scribano Y., Loreau J., Lique F., Feautrier N., 2020, MNRAS, 495, 2524
Barclay A., McKellar A., Moazzen-Ahmadi N., Dawes R., Wang X.-G., Carrington T., 2018, Phys. Chem. Chem. Phys., 20, 14431
Bop C. T., Batista-Romero F. A., Faure A., Quintas-Sánchez E., Dawes R., Lique F., 2019, ACS Earth Space Chem., 3, 1151
Brown J., Wang X.-G., Dawes R., Carrington T. Jr, 2012, J. Chem. Phys., 136, 134306
Brown J., Wang X.-G., Carrington T. Jr, Grubbs G. S., Dawes R., 2014, J. Chem. Phys., 140, 114303
Brünken S., Gupta H., Gottlieb C. A., McCarthy M. C., Thaddeus P., 2007, ApJ, 664, L43
Castro-Juárez E., Wang X.-G., Carrington T. Jr, Quintas-Sánchez E., Dawes R., 2019, J. Chem. Phys., 151, 084307
Cernicharo J., Guélin M., Agündez M., Kawaguchi K., McCarthy M., Thaddeus P., 2007, A&A, 467, L37
Cernicharo J., Guélin M., Agúndez M., McCarthy M. C., Thaddeus P., 2008, ApJ, 688, L83

Dalgarno A., McCray R. A., 1973, ApJ, 181, 95
Dawes R., Quintas-Sánchez E., 2019, in Parrill A. L., LipkowitK. B., eds, The Construction of Ab Initio-Based Potential Energy Surfaces, Reviews in Computational Chemistry, Chapt. 5. John Wiley & Sons, New Jersey, USA, p. 199
Dawes R., Wang X.-G., Jasper A. W., Carrington T. Jr, 2010, J. Chem. Phys., 133, 134304
Dawes R., Wang X. G., Carrington T., 2013, J. Phys. Chem. A, 117, 7612
Denis-Alpizar O., Stoecklin T., Halvick P., Dubernet M. L., 2013, J. Chem. Phys., 139, 034304
Denis-Alpizar O., Stoecklin T., Dutrey A., Guilloteau S., 2020, MNRAS, 497, 4276
Desrousseaux B., Quintas-Sánchez E., Dawes R., Lique F., 2019, J. Phys. Chem. A, 123, 9637
Desrousseaux B., Quintas-Sánchez E., Dawes R., Marinakis S., Lique F., 2021a, J. Chem. Phys., 154, 034304
Desrousseaux B., Lique F., Goicoechea J. R., Quintas-Sánchez E., Dawes R., 2021b, A&A, 645, A8
Donoghue G., Wang X.-G., Dawes R., Carrington T., 2016, J. Mol. Spectrosc., 330, 170
Dubernet M.-L. et al., 2013, A&A, 553, A50
Dumouchel F., Spielfiedel A., Senent M. L., Feautrier N., 2012, Chem. Phys. Lett., 533, 6
Green S., 1975, J. Chem. Phys., 62, 2271
Herbst H., 1981, Nature, 289, 656
Hutson J. M., Green S., 1994, MOLSCAT Computer Code, Version 14, Distributed by Collaborative Computational Project No. 6 of the Engineering and Physical Sciences Research Council (UK), available at https://www.theochem.ru.nl/molscat/Section1.html
Kawaguchi K. et al., 2007, PASJ, 59, L47
Kłos J., Lique F., 2011, MNRAS, 418, 271
Knizia G., Adler T. B., Werner H.-J., 2009, J. Chem. Phys., 130, 054104
Lara-Moreno M., Stoecklin T., Halvick P., 2019, MNRAS, 486, 414
McCarthy M. C., Gottlieb C. A., Gupta H., Thaddeus P., 2006, ApJ, 652, L141
McGuire P., Kouri D. J., 1974, J. Chem. Phys., 60, 2488
Massó H., Wiesenfeld L., 2014, J. Chem. Phys., 141, 184301
Quintas-Sánchez E., Dawes R., 2019, J. Chem. Inf. Model., 59, 262
Quintas-Sánchez E., Dawes R., Wang X.-G., Carrington T., 2020, Phys. Chem. Chem. Phys., 22, 22674
Remijan A. J., Hollis J. M., Lovas F. J., Cordiner M. A., Millar T. J., Markwick-Kemper A. J., Jewell P. R., 2007, ApJ, 664, L47
Sakai N., Sakai T., Yamamoto S., 2008, ApJ, 673, L71
Schöier F. L., van der Tak F. F. S., van Dishoeck E. F., Black J. H., 2005, A&A, 432, 369
Senent M. L., Hochlaf M., 2010, ApJ, 708, 1452
Senent M. L., Dayou F., Dumouchel F., Balança C., Feautrier N., 2019, MNRAS, 486, 422
Sobol I. M., 1976, USSR Comput. Math. Math. Phys., 16, 236
Thaddeus P., Gottlieb C. A., Gupta H., Brünken S., McCarthy M. C., Agúndez M., Guélin M., Cernicharo J., 2008, ApJ, 677, 1132
Walker K. M., Dumouchel F., Lique F., Dawes R., 2016, J. Chem. Phys., 145, 024314
Walker K. M., Lique F., Dumouchel F., Dawes R., 2017, MNRAS, 466, 831
Wang X.-G., Carrington T. Jr, Dawes R., 2016, J. Mol. Spectrosc., 330, 179
Werner H.-J., Knizia G., Manby F. R., 2011, Mol. Phys., 109, 407
Werner H.-J., Knowles P. J., Knizia G., Manby F. R., Schütz M., 2012, Wiley Interdiscip. Rev. Comput. Mol. Sci., 2, 242
Wernli M., Wiesenfeld L., Faure A., Valiron P., 2007, A&A, 464, 1147
Yazidi O., Ben Abdallah D., Lique F., 2014, MNRAS, 441, 664

This paper has been typeset from a TEX/LATEX file prepared by the author.